Stress-Free Two-Way Shape Memory Effect of Poly(ethylene glycol)/ Poly(epsilon-caprolactone) Semicrystalline Networks

Macromolecules

pubs.acs.org/Macromolecules

Article

Stress-Free Two-Way Shape Memory Effect of Poly(ethylene glycol)/Poly(ε-caprolactone) Semicrystalline Networks

Nicoletta Inverardi,* Maurizio Toselli, Giulia Scalet, Massimo Messori, Ferdinando Auricchio, and Stefano Pandini

Cite This: *Macromolecules* 2022, 55, 8533–8547

Read Online

ACCESS | Metrics & More | Article Recommendations | Supporting Information

ABSTRACT: In this work, poly(ethylene glycol) (PEG)/poly(ε-caprolactone) (PCL) semicrystalline networks were prepared by photo-cross-linking of methacrylated macromonomers with different molecular weights and in different proportions to obtain amphiphilic materials capable of displaying properly designed shape memory effects. Networks based on PCL 10 kDa and PEG 3 kDa showed suitable thermal and mechanical properties with well-separated crystallization and melting regions to achieve a self-standing two-way shape memory effect. Particularly, after the application of a specific thermomechanical history, these materials are capable of cyclically changing their shape between two configurations upon cooling–heating cycles in the absence of any external load applied. The effect of the composition of the networks and of the employed thermomechanical parameters, such as the applied strain and the actuation temperature, was investigated to shed light on the shape memory mechanism for this class of materials, which are considered promising for applications in the biomedical field and as reversible actuators for soft robotics.

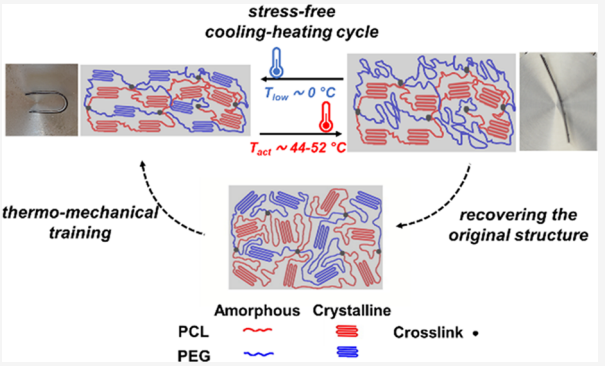

INTRODUCTION

Shape memory polymers (SMPs) have been widely studied thanks to their capability of providing large shape changes upon thermal transitions peculiar of their macromolecular structure. Traditionally, the most known and studied effect is the so-called "one-way shape memory effect" (SME), which involves the unidirectional/irreversible change between a temporary shape and a permanent one.[1,2] To provide reversibility to the effect, and therefore the possibility to repetitiously and bidirectionally change between two given shapes, the "two-way" SME was investigated and obtained thanks to the rational use of cooling and heating cycles under the presence of an external load in semicrystalline polymeric networks. More in details, it was observed that for these networks, heated above their melting temperature and in the presence of an external tensile load, a significant elongation occurs upon crystallization.[3−5] This crystallization-induced elongation (CIE) may be almost completely recovered upon subsequent melting, and the deformation changes may be repetitiously obtained by employing the on/off thermal stimulus. Starting from the first evidence of the two-way SME reported for a cross-linked poly(cyclo octene) by Chung et al.[3] in 2008, for a poly(ε-caprolactone) (PCL)-based shape memory polyurethane by Hong et al.[6] in 2010, and in the same year, for a multiphase polymeric network containing polypentadecalactone and PCL by Zotzmann et al.,[7] several interesting works were carried out to elucidate the physics behind, derive structure–property correlations, and optimize the effect. In fact, various thermodynamic and/or thermomechanical descriptions and modeling of the effect were developed[5,8,9] together with the synthesis of novel materials for tuning such an effect.[10−14] Furthermore, the influence of material architecture on this effect was studied, for example, using various macromolecular architectures (e.g., linear, three-arm, and four-arm branched macromonomers)[15] or by varying the cross-link density while keeping the degree of crystallinity almost constant[16] and by cross-linking melt-blended systems.[17,18]

Recently, the possibility of achieving reversible shape changes upon cooling–heating cycles without the need of an external load, also referred to as "reversible" or "stress-free two-way" SME, was demonstrated for specific classes of SMPs. In such SMPs, the effect is achieved by means of two domains in the material architecture: (i) an actuation domain and (ii) a structural domain. The first domain is responsible for the classical CIE due to crystallization. The second domain provides the internal driving force necessary for the CIE of

Received: May 22, 2022
Revised: August 29, 2022
Published: September 22, 2022

https://doi.org/10.1021/acs.macromol.2c01064
Macromolecules 2022, 55, 8533–8547

the first domain under a stress-free condition. There exist multiple strategies for the preparation of such SMPs, which can be divided into three categories based on the employed macromolecular architecture: (i) semicrystalline polymer networks with a broad melting region, (ii) multiphase semicrystalline networks, and (iii) networks obtained by a secondary postcuring treatment performed on a stretched structure. The first category, the most investigated one together with the third,[19,20] may be employed by partially melting the cross-linked structure, so to divide the melting peak into a part consisting of a skeleton domain (i.e., crystals at high temperature providing an internal driving force) and in another one, which is the actuator domain (i.e., crystals for lower temperature, which cyclically melt and crystallize). To this end, a series of copolymer networks based on oligo(ε-caprolactone) and *n*-butyl acrylate (BA) were purposely synthesized to show a broad melting region in a temperature range close to the human body temperature.[21] Similarly, using poly(ethylene glycol) (PEG) of different molecular weights and BA, Yang et al. obtained a broad melting region leveraged to achieve a reversible deformation under tensile conditions of about 8% between the body temperature and 0 °C.[22] The achievement of a broad melting region thanks to the use of cross-linked copolymer networks was also found to be useful to provide temperature-memory and bidirectional actuation over large cycle numbers.[23] Furthermore, also monophasic systems with an enough broad melting region may behave similarly, allowing one to obtain a two-way reversible response, reaching values above 10% reversible strain, under stress-free conditions.[24−28] The second of the aforementioned categories harnesses two separate crystallizable domains to achieve the stress-free SME and was proposed for the first time in 2013. In fact, in the pioneering work by Behl et al., the low-melting-point phase (PCL) represented the actuator domain, whereas the high-melting-point phase (poly(ω-pentadecalactone)) represented the skeleton providing the internal force.[29] The choice of dealing with two separate phases for the two different domains is advantageous with respect to the materials of the first category for what concerns the possibility of having a fixed actuation temperature or temperature window that can reliably activate the phenomenon. In fact, if the two melting regions of the two domains are separated well-enough, it becomes easy from an experimental point of view to provide the suitable activation temperature. On the contrary, the actuation temperature in the case of SMPs with a broad melting region (i.e., the first category) has to be carefully controlled; otherwise, it may result in the complete melting of the skeleton or not enough to produce a clear effect. However, in multiphase polymer systems with more than one crystallizable block, both thermal properties and crystallization are strongly dependent on the degree of miscibility between components, prepolymer molar mass, thermal history, and processing conditions. This is probably why the strategy based on the preparation of two-way reversible shape memory polymers from multiphase copolymer networks/blends has not yet been widely explored, with only few but interesting works reported.[30−33]

In the literature, the miscibility and the crystallization of PCL/PEG blends and PCL−PEG block copolymers have been extensively analyzed and reported. Briefly, Qiu et al. investigated the miscibility and crystallization by means of phase-contrast microscopy and claimed that high-molecular-weight PEG (M_w = 100 kDa), i.e., poly(ethylene oxide), is not miscible with PCL.[34] Conversely, Kuo et al. observed miscibility between PEG and PCL, comparing the crystallization temperature in the blends with those of the homopolymers,[35] and the presence of a miscibility window of upper critical solution temperature (UCST) character has been widely proposed.[36−38] For instance, Nguyen-Tri and Prud'homme studied the isothermal crystallization behavior and phase separation of PCL/PEG (50/50) blends with close melting temperatures.[38] It was observed that at a low temperature (30 °C, which is below the UCTS), there is a phase separation in the melt and PCL forms spherulites, while PEG crystallizes in a second step on the spherulitic boundary. Conversely, at a higher crystallization temperature (40 °C, which is above the UCST), where the phase separation has not taken place yet, the two polymers crystallize simultaneously with internal phase separation during the crystallization. Also, the morphology, crystal structure, and crystallization behavior of PCL-*b*-PEG diblock and PCL-*b*-PEG-*b*-PCL triblock copolymers have been studied, and several reports and reviews have been published on this matter.[39−44] These block copolymers exhibit miscibility in the melt and form PCL and PEG crystals in a wide composition range with no eutectic crystal of the two components.[41−43] The crystallization of the blocks is affected by the composition, block molecular weight, and molecular architecture of the copolymer. Piao et al. demonstrated that in PCL-*b*-PEG-*b*-PCL copolymers, the crystallization of the PEG block is restricted by the earlier crystallization of PCL blocks that are covalently coupled to the two ends of the PEG block.[43] Both crystallization and melting of PCL and PEG can overlap depending on the molecular weight of each component, but as expected, the melting and crystallization temperatures of PCL and PEG blocks decrease with decreasing molecular weight of the block. He et al. characterized the morphology and the crystallization behavior of PCL-*b*-PEG copolymers.[41,44] It was concluded that the relative block length determines the order of block crystallization. More in details, when the length of the PCL block is longer, it crystallizes first, leading to imperfect crystallization of the PEG block and vice versa.

In this work, we synthesized PCL-*b*-PEG copolymer networks with two different crystalline phases characterized by well-separated melting and crystallization transitions. The semicrystalline networks were prepared by photo-cross-linking of methacrylate-terminated PCL and PEG with different molecular weights and in different proportions. A preliminary study was performed by mainly analyzing the thermal properties of the networks with different molecular weights and with various proportions of the two components to find the molecular structures with optimal and/or tunable thermal properties for the intended SME. The final aim was to build on the knowledge of their peculiar macromolecular structure to obtain a reliable stress-free two-way SME. A thorough investigation on the response of three selected formulations was then performed. Their two-way SME under stress and stress-free conditions was quantitatively assessed, with particular attention to the effect of the composition of the material and the thermomechanical parameters applied during the shape memory cycles, such as the prestrain and the actuation temperature.

EXPERIMENTAL SECTION

Materials. PEGs with different average molecular weights of M_n = 2 kDa (PEG2), 3 kDa (PEG3), and 4 kDa (PEG4), PCL diol (M_n ~

https://doi.org/10.1021/acs.macromol.2c01064
Macromolecules 2022, 55, 8533−8547

10 kDa, PCL10), 2-isocyanatoethyl methacrylate (2-IEM, 98%), tin(II) 2-ethylhexanoate, and tetrahydrofuran (THF) were purchased from Sigma-Aldrich and used as received without any further purification. The photoinitiator is 2-hydroxy-2-methyl-1-phenyl propanone (Additol HDMAP) purchased from Cytec.

Synthesis of Dimethacrylated Macromonomers. The methacrylation of the hydroxyl end groups of PCL and PEGs with 2-IEM was conducted according to the protocol reported in the literature.[45] After drying the polymer at 60 °C under dynamic vacuum in the presence of molecular sieves, methacrylate end-capping of hydroxy-terminated PCL and PEGs was carried out by reacting them with 2-IEM in bulk at 100 °C for about 3−4 h in the presence of an organotin catalyst. The reaction was monitored by IR until the ratio of peak strength at 2930−2275 cm^{-1} became constant. 2-IEM was added with a 20% stoichiometric excess with respect to hydroxyl groups of the diol macromonomers. Unreacted 2-IEM was removed by dynamic vacuum at the end of the reaction, and Fourier-transform infrared spectroscopy (FT-IR) was performed to ensure the absence of 2-IEM, which is confirmed by the lack of the signal corresponding to the isocyanate group at 2275 cm^{-1}. The methacrylation of PEG3 can be taken as an example: 30.0 g of PEG (10 mmol) was introduced into a glass flask previously flushed with nitrogen followed by 3.72 g of 2-IEM (24 mmol) and using tin(II) 2-ethylhexanoate as a catalyst (0.060 g). The reaction was carried out under a nitrogen atmosphere and mechanical stirring for about 3−4 h.

Preparation of Chemically Cross-Linked Networks. PCL and PEG dimethacrylates were carefully melt-mixed at 80 °C in the proper ratio; then, Additol HDMAP was added as a radical photoinitiator (0.1 wt %). The well-mixed melts were poured into a mold formed of two glass plates (25 mm × 75 mm) and Teflon spacers (thickness: 1.2 and 0.3 mm). Photo-cross-linking was performed on a heated plate under 365 nm UV irradiation (Hamamatsu LC8 spot light source) at 12 cm above the sample (intensity 6 mW cm^{-2}) for 5 min on both sides. Free films with thicknesses of about 1.5 mm and 400 μm were obtained by peeling them from the glass plate and completing the curing process by irradiating further for 5 min on each side.

Chemical Characterization. FT-IR spectroscopy was performed using a PerkinElmer FT-IR system Spectrum Two operating in the attenuated total reflection (ATR) mode. A total of 32 scans with a resolution of 4 cm^{-1} were carried out. ^{1}H NMR spectra were recorded in $CDCl_3$ at 400 MHz with a Mercury 400 spectrometer. Chemical shifts were referred to tetramethylsilane at 0 ppm.

Material Characterization. The thermal properties of all networks were investigated by differential scanning calorimetry (DSC). The preliminary analyses were performed at 10 °C min^{-1} with heating/cooling/heating scans in the −60/80 °C temperature region on a DSC Q10 (TA Instruments). The crystallinity content of PCL and PEG domains was calculated according to the following equation

$$\chi_{c,i} = \frac{\Delta H_{m,i}}{\Delta H_{m,i}^{100}} \cdot \frac{1}{w_i} \tag{1}$$

where $\Delta H_{m,i}$ is the melting enthalpy of the i-phase (PEG or PCL) in the second heating scan, $\Delta H_{m,i}^{100}$ is the specific melting enthalpy for the 100% crystalline i-phase (i.e., equal to 205 J g^{-1} for PEG[46] and 135 J g^{-1} for PCL[47]), and w_i is the weight percentage of the i-phase (PEG or PCL) in the network. On three selected compositions (i.e., PCL10PEG3 2:1, 1:1, and 1:2), a further DSC test was performed at a lower rate equal to 2 °C min^{-1}, with heating/cooling/heating scans on the same thermal region. The selected networks were also characterized in terms of gel fraction and swelling ratio. Specimens with initial mass m_0 and shape 20 × 20 × 0.4 mm^3 were placed in 20 mL of THF at room temperature. The mass of the swollen specimen (m_s) was determined after about 24 h. After that, the swollen sample was dried at room temperature until a constant weight to measure the residual mass of the sample after extraction (m_d). The degree of swelling (Q) and the gel content (G) were calculated according to the following equations

$$Q = 1 + \frac{\rho_1}{\rho_2}\left(\frac{m_s}{m_d} - 1\right) \tag{2}$$

$$G = \frac{m_d}{m_0} \tag{3}$$

where ρ_1 and ρ_2 are the densities of THF (0.889 g cm^{-3}) and the film network (assumed as 1.12 g cm^{-3}, value calculated based on amorphous and crystalline phase densities of the two homopolymers).

Water uptake measurements were performed on samples with various PCL10−PEG3 compositions. Films ranging from 200 to 250 mg were soaked in distilled water for 24 h at room temperature. Surfaces of the samples were gently dried with a tissue paper, and the mass of each sample was weighed. Water uptake was defined as the ratio of the wet weight to dry weight.

Dynamic-mechanical thermal analysis (DMTA) was carried out by means of a DMA Q800 (TA Instruments) on rectangular strips (gauge length: 10 mm; width: about 5 mm) under tensile conditions. Each specimen was subjected to the application of an oscillating displacement of 15 μm amplitude at 1 Hz under a thermal ramp between 65 and −20 °C at 2 °C min^{-1} under a cooling/heating cycle.

The mechanical behavior of the networks in their rubbery plateau was studied on rectangular strips (gauge length: 10 mm; width: about 5 mm) in tensile tests, carried out at 65 °C on the DMA Q800 under the tensile configuration at a testing rate of 1 N min^{-1} on at least three samples for each material.

The two-way shape memory behavior was investigated on rectangular strips (length between grips: 10 mm, width: about 5 mm) by means of the DMA Q800 in the tensile mode under three different testing protocols to explore the influence of various thermomechanical parameters.

In the first protocol, a tensile deformation equal to 20% was applied to the specimens at 65 °C and the shape memory behavior was studied under cooling−heating cycles under a constant stress (corresponding to the 20% strain) between −20 and 65 °C at 2 °C min^{-1}. Then, in the following protocols, the stress-free reversible SME was investigated with the aim of understanding the effect of the applied prestrain and that of the actuation temperature of the cycle.

In the second protocol, a tensile prestrain of a given amount (10, 20, 30, and 40%) was applied at 65 °C and a cooling step under fixed stress conditions (corresponding to the level of deformation achieved in the previous step) was performed at 2 °C min^{-1} down to −20 °C. Then, the specimen was unloaded (down to a minimum load equal to 0.001 N) and heated under quasi-stress-free conditions at a constant heating rate of 2 °C min^{-1} up to the actuation temperature (T_{act}) equal to 43 °C; then, the reversible strain cycle was measured along a cooling/heating cycle at 2 °C min^{-1} in the −20/65 °C temperature region. In a further test, to evaluate the repeatability of the effect, three subsequent stress-free cooling/heating cycles were performed at 2 °C min^{-1} in the −15/43 °C temperature region.

Finally, in the third protocol, the effect of T_{act} was investigated on specimens that underwent a prestrain equal to 20% and a subsequent cooling step at 2 °C min^{-1} down to −20 °C, in the presence of the constant stress achieved at the end of the prestrain step. Such prestretched specimens were then unloaded (down to 0.001 N) and heated at a constant heating rate of 2 °C min^{-1}. Three subsequent cooling/heating cycles were performed corresponding to three different T_{act}, namely, 32, 42, and 50 °C, at a cooling/heating rate equal to 2 °C min^{-1}.

The self-standing two-way SME was also investigated on 50 mm-long bars (cross section: 5 mm × 1.5 mm), which were programmed under folding conditions at 65 °C in a U-shape, fixed by cooling under the imposed shape at −20 °C. The self-standing two-way SME of the thus-programmed samples was measured under both dry and wet conditions. Under dry conditions, the sample was (i) heated for 5 min at T_{act} by placing it on a stainless steel plate inside the furnace of the dynamic-mechanical analyzer, which is capable of maintaining the set temperature reliably; (ii) removed to cool it down inside a freezer at −20 °C (below the crystallization temperature of both phases, thereafter called T_{low}); steps (i) and (ii) were repeated for various T_{act}

https://doi.org/10.1021/acs.macromol.2c01064
Macromolecules 2022, 55, 8533−8547

Scheme 1. Methacrylate Functionalization of Hydroxyl-Terminated PCL and PEG, and Scheme of the Network Structure after UV Cross-Linking

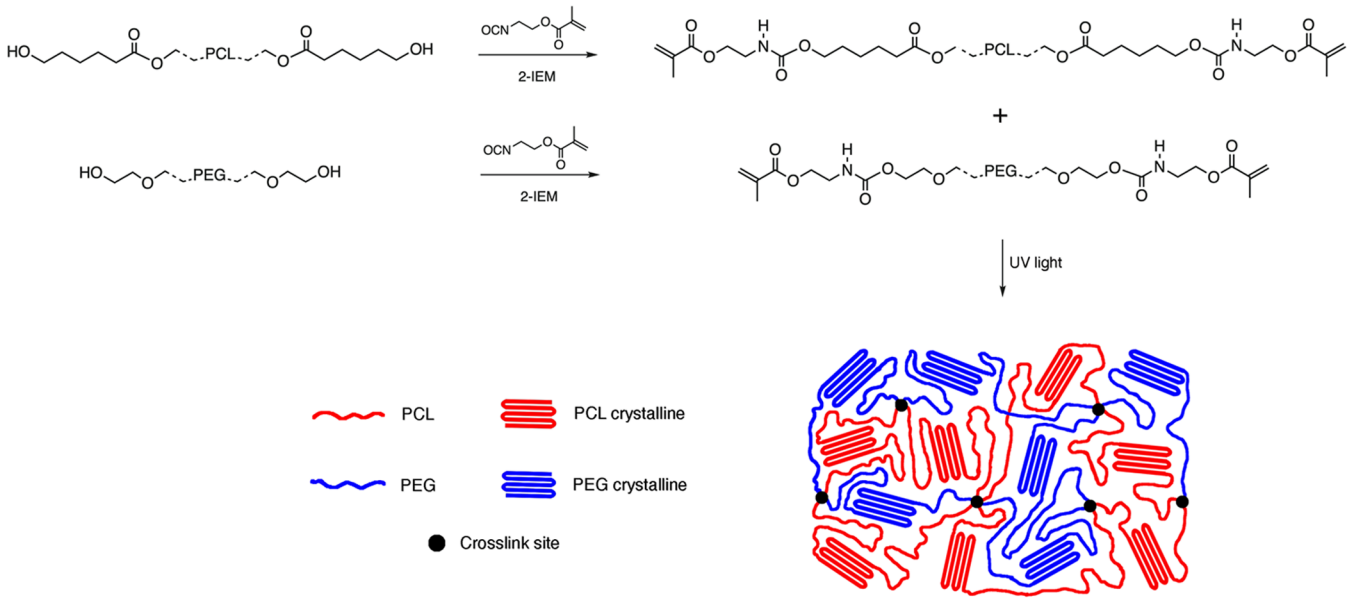

Table 1. Thermal Analysis of Semicrystalline Networks (DSC at 10 °C min^{-1})

	preliminary DSC tests (10 °C min^{-1})									
material code	$T_{c,PEG}$ (°C)	$T_{c,PCL}$ (°C)	$T_{m,PEG}$ (°C)	$T_{m,PCL}$ (°C)	$\Delta H_{c,PEG}$ (J g^{-1})	$\Delta H_{c,PCL}$ (J g^{-1})	$\Delta H_{m,PEG}$ (J g^{-1})	$\Delta H_{m,PCL}$ (J g^{-1})	$\chi_{c,PEG}$ (%)	$\chi_{c,PCL}$ (%)
PCL10		8		42		39		39		30
PEG2	−30		17		27		32		19	
PEG3	−4		29		50		52		28	
PEG4	5		32		59		59		31	
PCL10PEG2 2:1	−39	4	10	40	n.e.[a]	23	6	17	10	19
PCL10PEG2 1:2	−39	6	8	40	8	8	16	6	13	14
PCL10PEG3 2:1	−9	8	26	42	15	17	13	12	21	14
PCL10PEG3 1:2	−8	10	27	42	31	7	30	5	24	12
PCL10PEG4 2:1	−3	6	32	41	14	24	14	19	22	22
PCL10PEG4 1:2	2	7	31	41	30	6	30	5	24	12

[a]Not evaluable.

values in the range 39−52 °C. On the other hand, for recovery experiments performed by immersion into water, the programmed sample was immersed in a temperature-controlled water bath at various T_{act} values ranging from 40 to 45 °C and equilibrated at this temperature for at least 2 min. Afterward, it was immersed and equilibrated in a temperature-controlled cooling bath at a temperature well below the crystallization temperature (T_{low} is about 4 °C). Subsequent immersion in heating and cooling baths was performed cyclically. The temperature of the water baths was continuously monitored with a thermocouple placed near the sample. For both conditions of recovery, at each step, shape changes were recorded by means of a camera (Nikon D700) and pictures were processed by a software (ImageJ) for the evaluation of the change in the angle.

RESULTS AND DISCUSSION

Synthesis and Preliminary Characterization of PCL-PEG Networks. The photo-cross-linkable macromonomers were synthesized according to a protocol described in the literature[45] through the reaction of PCL and PEG diols with 2-IEM (Scheme 1).

The ^{1}H NMR spectra confirmed the reaction of 2-IEM and showed the conversion of hydroxyl end groups of PCL and PEGs with the formation of the expected methacrylated macromonomers. The ^{1}H NMR spectra of PCL10 and PEG3 methacrylated macromonomers in comparison with the respective pristine polymers are reported in Figures S1 and S2 (Supporting Information).

Subsequently, semicrystalline networks were obtained by photo-cross-linking of PCL10 with PEG2, PEG3, and PEG4 diacrylates at different weight ratios of 1:2, 1:1, and 2:1. The results of preliminary thermal analysis of these PCL−PEG networks compared with the UV-cured methacrylated homopolymers are reported in Table 1 and Figures S3−S5 (Supporting Information).

Interestingly, at a rate of 10 °C min^{-1}, the cross-linked PCL10-based network shows a melting temperature, T_m, of 42 °C, a crystallization temperature, T_c, of 8 °C, and an enthalpy of crystallization, $\Delta H_{c,PCL}$, equal to 39 J g^{-1}. These data confirm the trend already reported in the literature by which cross-linked PCL presents a lower crystalline fraction and transition temperatures T_m and T_c with respect to PCL diacrylate, which has T_m of 58 °C, T_c of 28 °C, and enthalpy of crystallization equal to 62 J g^{-1}, as measured at the same heating/cooling rate and under the same experimental conditions (Figure S4, Supporting Information). In the case

https://doi.org/10.1021/acs.macromol.2c01064
Macromolecules 2022, 55, 8533−8547

of all of the other curves being reported, which correspond to copolymeric networks of PCL10 with varying molecular weights of PEG (i.e., PEG4, PEG3, and PEG2), the presence of more than one endothermal/exothermal signal can be observed both in the heating scan and in the cooling scan, testifying the presence of a multicrystalline structure.

Peaks related to melting and crystallization are well evident and, in most of the cases, they are easy to correlate to their relevant polymeric phase. In fact, by comparing the T_m measured for the components to the melting peaks found for the multiphase networks, the PCL phase is easy to locate as the high-melting-point phase with T_m approximately equal to 40−42 °C in all of the networks, whereas the PEG phase can be recognized as the low-melting-point phase in PCL−PEG networks based on PEG2, PEG3, and PEG4 diacrylates. More in details, for photo-cross-linked PEGs with increasingly greater molecular weight, the T_m shifts to a higher temperature (i.e., from 17 to 32 °C, passing from PEG2 to PEG4; Table 1 and Figure S5), and this trend is found also for the copolymeric networks in which $T_{m,PEG}$ moves from 8 to 32 °C. As already reported in the literature,[41,44] the first phase to crystallize is known to be the one with a longer block length/molecular weight; thus, the difference in block length between PCL10 and PEG2/PEG3/PEG4 may be regarded as significant. In all of the networks, $T_{m,PCL}$ and $T_{c,PCL}$ are about 40 °C and in the range of 5−10 °C, respectively, regardless of the composition. On the contrary, the crystallinity content for the PCL phase, $\chi_{c,PCL}$, appears to be strictly dependent on the composition and is affected by the presence of the PEG phase. The crystallinity content was calculated according to eq 1, in which the specific melting enthalpy for the 100% crystalline phase is weighed based on the percentage of the phase itself. More in details, $\chi_{c,PCL}$ decreases from 30%, which is the value measured for the pure cross-linked PCL, to about 12−22% for the PCL−PEG networks (Table 1). For what concerns the PEG phase in the copolymeric networks, its melting and crystallization temperatures are approximately in line with the temperatures measured for its respective cross-linked diacrylate macromonomer. However, the crystallization of the PEG phase is partially hindered by the presence of PCL, resulting in the crystallinity content $\chi_{c,PEG}$ being significantly smaller than those measured for the diacrylate ones. By way of example, in the 1:2 compositions, which are the PEG-dominated networks, hence with a higher crystallinity content, $\chi_{c,PEG}$ is equal to 13, 24, and 24% for PCL10PEG2, PCL10PEG3, and PCL10PEG4, respectively, compared to 19, 28, and 31% for pure cross-linked PEG2, PEG3, and PEG4, respectively. Furthermore, these preliminary DSC results are very useful to select promising materials for the self-standing two-way SME. In fact, as discussed before, for biphasic systems, there should exist two domains that have to address two specific functions: the one with the higher transition temperature represents the skeleton domain, which provides the internal/structural driving force for the CIE, whereas the one with the lower transition temperature is the switching domain, which cyclically melts and crystallizes to obtain the change in macromolecular mobility required for the shape changes. Additionally, the two domains should be distant enough on the temperature scale with a significant separation between the melting and crystallization zones of the two phases. In this respect, the differences between $T_{m,PCL}$ and $T_{m,PEG}$ are about 10, 15, and 28 °C and the differences between $T_{c,PCL}$ and $T_{c,PEG}$ are about 8, 17, and 40 °C, for PCL10PEG4, PCL10PEG3, and PCL10PEG2, respectively. Therefore, it may be difficult to identify an optimal actuation temperature in between the melting of the PEG and PCL phases for PCL10PEG4 networks, as is evident also from the partial overlapping of the relevant peaks in Figure S3 (Supporting Information). On the contrary, for PCL10PEG2 networks, the temperature window on which the phases are distributed is very wide and may be difficult to reach from an experimental point of view. Even more importantly, PCL10PEG2 networks show a brittle mechanical behavior with elongation at break smaller than 35%, as measured in preliminary tensile tests carried out in the rubbery plateau at 65 °C (Figure S6, Supporting Information). Therefore, the selected compositions for the intended SME are those based on PCL10−PEG3, and the following characterizations were performed on PCL10PEG3 2:1, 1:1, and 1:2 networks.

Thermal and Physical Properties of Networks. Thermal analysis on the three selected networks was performed by means of DSC scans carried out at 2 °C min^{-1}, which is the same heating/cooling rate applied for the shape memory tests later described. The results of the DSC scans are shown in Figure 1 and listed in Table 2. The

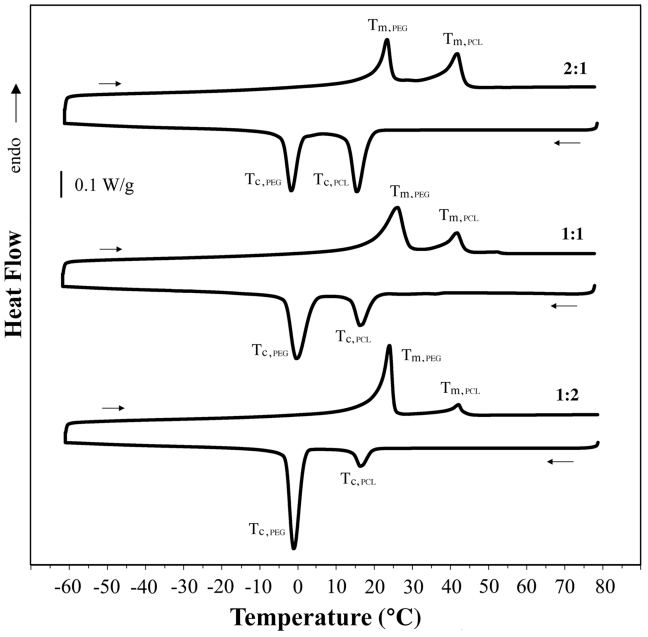

Figure 1. DSC cooling and second heating scans at 2 °C min^{-1} of PCL10PEG3 networks.

Table 2. Thermal and Physical Characterization of PCL10PEG3 Semicrystalline Networks (DSC at 2 °C min^{-1})

	DSC tests (2 °C min^{-1})					
material code	$T_{c,PEG}$ (°C)	$T_{c,PCL}$ (°C)	$T_{m,PEG}$ (°C)	$T_{m,PCL}$ (°C)	G^a (%)	Q^b (%)
PCL10PEG3 2:1	−1	17	23	43	94	225
PCL10PEG3 1:1	0	17	26	43	90	212
PCL10PEG3 1:2	−2	18	24	43	91	195

[a] G, gel fraction. [b] Q, swelling ratio.

https://doi.org/10.1021/acs.macromol.2c01064
Macromolecules 2022, 55, 8533−8547

networks with varying proportions between the PEG3 and PCL10 phases reveal two distinct melting and crystallization peaks.[48] As expected, the effect of the lower cooling rate with respect to the one adopted for the preliminary DSC analysis results in a narrowing of the peaks and in shifting the crystallization under cooling toward higher temperatures (i.e., $T_{c,PEG}$ moves from about −8 °C to about 0 °C and $T_{c,PCL}$ moves from about 10 to 18 °C when lowering the cooling rate from 10 to 2 °C min^{-1}), whereas the melting temperatures and enthalpies under heating remain essentially unchanged.

Furthermore, all of the networks present high values of gel content (G = 90−94%) and relatively low values of swelling ratio, indicating the achievement of an efficient cross-linked structure after the UV curing process. Among the three compositions, PCL10PEG3 1:2 is expected to have the highest degree of cross-linking, given the lowest value of the swelling in THF. This may be expected since the 1:2 composition is the one with a higher percentage of the PEG phase, which is the short-chain phase. Thus, it may be reasonable that it has the highest number of terminal methacrylate groups where the cross-linking reaction takes place.

Thermomechanical and Mechanical Properties of Networks. DMTA analyses were performed to investigate the thermomechanical properties of the networks, with particular reference to the evolution of the storage modulus, E', as a function of temperature, and to investigate the presence of a rubbery plateau above melting, which indirectly evidences the cross-linked structure. The tests were performed starting from temperatures above melting and performing a controlled cooling below the crystallization temperature of both phases and a subsequent heating up to above melting to characterize both crystallization and melting phenomena. The results are shown in Figure 2, and the evaluation of the storage modulus at different temperatures together with an estimation of the cross-link density is listed in Table 3.

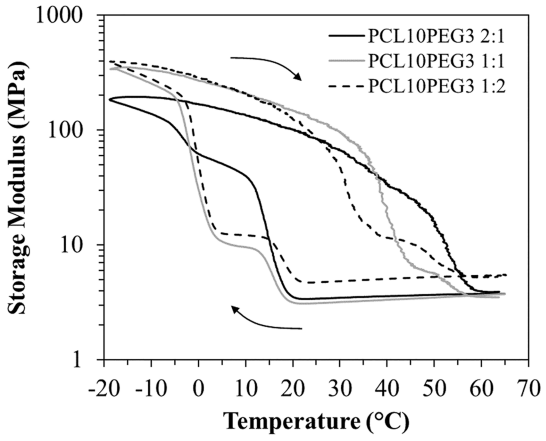

Figure 2. Storage modulus as a function of temperature on a cooling−heating cycle for PCL10PEG3 networks.

At the highest temperature explored, all of the networks are in their rubbery plateau with an almost constant value of the rubbery storage modulus. Upon cooling, it is possible to clearly notice the separate effect of the crystallization of the two phases occurring in the 5/20 °C temperature interval and the −20/5 °C temperature window for the PCL10 and the PEG3 phases, respectively. With the first crystallization, a step increase in the value of the storage modulus occurs and its absolute value is found to be dependent on the network composition. In fact, as the proportion of the PCL10 phase in the networks increases from PCL10PEG3 1:2 and 1:1 to 2:1, the measured increment of E' at 10 °C goes from about 7 MPa to about 36 MPa. Similarly, for the subsequent step increase, the measured E' is maximum for PCL10PEG3 1:2 (about 380 MPa) and PCL10PEG3 1:1 (about 360 MPa) and much lower for PCL10PEG3 2:1 (about 140 MPa), reflecting the increasingly smaller degree of crystallinity for the PEG3 phase from PCL10PEG3 1:2 to 2:1. Upon heating, the three networks show an even more different response. In fact, for PCL10PEG3 1:2, a first quite smooth decrease in the storage modulus ascribed to the melting of the PEG3 phase occurs in a temperature region evaluated between 20 and 40 °C, followed by another distributed decrease due to the melting of PCL10 crystals down to the value of the rubbery modulus, equal to 5.5 MPa at 65 °C. For the case of PCL10PEG3 1:1, the melting zone for the PEG3 phase appears to be slightly more distributed and finishing to decrease at about 45 °C, where the second melting occurs and eventually leads to the value of the rubbery plateau equal to 3.5 MPa. Finally, for the PCL10PEG3 2:1 network, a smoother curve is reported, where the separation between the melting of the two phases is less visible and can be only appreciated by looking at the inflection point present at about 45 °C. These results are well in agreement with the ones from DSC tests. Notwithstanding the differences in the analyses themselves, it is possible to confirm the location of the various phase transitions. Furthermore, thanks to DMTA analyses, it was easier to evaluate the distribution of the melting processes, with specific reference to the effect of the crystal presence on the mechanical behavior of the material. In particular, two well-separated melting subprocesses were found for PCL10PEG3 1:2 and 1:1 networks, with a more distributed process for the melting of the PEG in PCL10PEG3 1:1, confirming the broader breadth of the first endothermic peak from DSC depicted in Figure 1. On the contrary, a much less evident separation between the two melting processes was observed for PCL10PEG3 2:1, in agreement with DSC data. In fact, from the thermal DSC heating scan, the onset of the melting for PCL10 seems to start at a lower temperature of about 35 °C, making the two melting processes partially overlapping.

Furthermore, the presence of a plateau above 60 °C indicated the proper achievement of a cross-linked structure. For a first evaluation of the cross-linking density, the rubber theory was applied with eq 4

$$E = 3\nu RT \tag{4}$$

where E is the material modulus in the rubbery region, here approximated with the value of E' at 65 °C, R is the universal gas constant, T is the absolute temperature, and ν is the cross-linking density defined as moles per unit volume. The cross-linking density was found to be slightly higher in the case of the PCL10PEG3 1:2 network, consistent with the presence of PEG3 as the main component, as already noted for the swelling experiments. In fact, since PEG3 has a low molecular weight and thus also a low chain length, there are more methacrylate groups available for the cross-linking reaction.

Additionally, the mechanical behavior of the systems in the rubbery plateau was investigated by tensile tests at 65 °C, carried out by means of a dynamic-mechanical analyzer. The results of the stress−strain curves are shown in Figure 3, and the evaluation of material properties is listed in Table 3. These

https://doi.org/10.1021/acs.macromol.2c01064
Macromolecules 2022, 55, 8533−8547

Table 3. Results of the Thermomechanical Characterization and of the Tensile Tests Performed at the Deformation Temperature, T_{def}

	DMTA tests					tensile tests at T_{def}[a]			
material code	E' at −20 °C (MPa)	E' at 10 °C (MPa)	E' at 45 °C (MPa)	E' at 65 °C (MPa)	cross-link density, after E' (mol cm^{-3})	E (MPa)	cross-link density, after E (mol cm^{-3})	σ_b (MPa)	ε_b (%)
PCL10PEG3 2:1	175	39.6	25.0	3.7	4.4×10^{-4}	4.8 ± 0.2	$(5.7 \times 10^{-4}) \pm (0.2 \times 10^{-4})$	2.4 ± 0.1	96 ± 14
PCL10PEG3 1:1	366	9.8	7.3	3.5	4.2×10^{-4}	5.7 ± 1.0	$(6.8 \times 10^{-4}) \pm (1.2 \times 10^{-4})$	1.3 ± 0.2	39 ± 7
PCL10PEG3 1:2	395	12.1	10.8	5.5	6.5×10^{-4}	6.0 ± 0.7	$(7.1 \times 10^{-4}) \pm (0.8 \times 10^{-4})$	2.7 ± 0.6	70 ± 13

[a]Average and standard deviations are reported for tensile tests (n = 3).

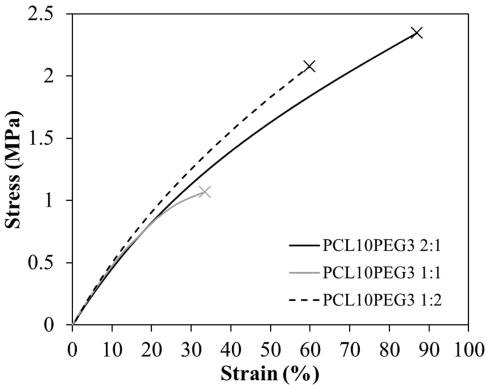

Figure 3. Stress versus strain curves measured under tensile conditions at 65 °C. For each network, only one representative curve was represented (on at least three samples tested).

test results allowed us to better evidence the effect of the PEG3 content on the tensile modulus. In fact, the stiffness, and consequently, also the cross-linked density, was found to be greater for networks with more PEG3, apparently following a linear fashion.

Mechanical testing is also fundamental to evaluate the strain and stress at break, which are important parameters for the design of shape memory testing. In particular, from the strain at break, it is possible to determine the maximum safe strain that can be applied during the deformation step in the shape memory protocol, without failure. PCL10PEG3 2:1 was found to be the most extensible network with an elongation at break of around 100%. Actually, PCL10 was chosen to provide a well-separated melting temperature with respect to PEG3 but also to increase the extensibility of the overall networks, in light of the recognized quite brittle behavior of PEGs. The most brittle network was for PCL10PEG3 1:1, with an elongation at break of about 35%, whereas PCL10PEG3 1:2 allowed applying of a significant deformation without tensile failure (elongation at break equal to about 70%).

Two-Way Shape Memory Characterization of Networks. The two-way shape memory behavior was studied to investigate the possibility of reversible shape changes both with and without the presence of a mechanical load for the selected networks. To this aim, we first characterized the response of the networks under the traditionally employed two-way shape memory protocol, which involves the presence of a constant applied load. This characterization was carried out by means of the dynamic-mechanical analyzer by first applying a tensile prestrain at a deformation temperature, T_{def} = 65 °C, within the rubbery plateau for all of the networks. Furthermore, a deformation of about 20%, which is well below the strain at break for all of the systems as reported in Table 3, was applied to structure all of the macromolecular networks similarly. Due to the slightly different stiffness of the networks, an increasingly greater stress was required to achieve a 20% deformation when increasing the content of the PEG3 phase (i.e., from 860 to 1190 kPa, approximatively). While holding the applied stress constant, a cooling/heating cycle at a controlled rate was carried out to promote and evaluate the reversible strain change stemming from the CIE and the consequent melting-induced contraction.

Two parameters were introduced to quantitatively characterize the two-way shape memory behavior, defined as the actuation magnitude, AM, and the recovery magnitude, RM[3]

$$\text{actuation magnitude, AM} = (\varepsilon_{low} - \varepsilon_{applied}) \times 100 \quad (5)$$

$$\text{recovery magnitude, RM} = \frac{\varepsilon_{low} - \varepsilon_{high}}{\varepsilon_{low} - \varepsilon_{applied}} \times 100 \quad (6)$$

where ε_{low} is the deformation evaluated at −20 °C, $\varepsilon_{applied}$ is the deformation applied at 65 °C (20% nominal), and ε_{high} is the recovered deformation obtained at the end of the heating ramp at 65 °C. The actuation magnitude describes the final evolution of strain taking place during cooling at the end of the crystallization process, whereas the recovery magnitude represents the percentage of strain that was attained during cooling, recovered at the end of the subsequent heating. From an applicative point of view, AM is useful to understand the extent of change in strain that can be exploited upon crystallization and RM gives an idea of how efficient the recovery process of the deformation is.

Results of the two-way shape memory tests following the aforementioned protocol are shown in Figure 4. The strain versus temperature curves for all of the materials clearly evidenced the evolution of the strain as a consequence of the

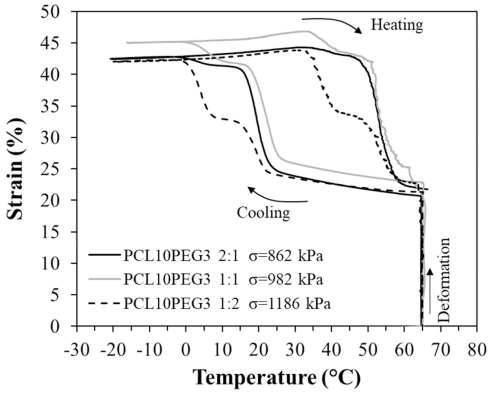

Figure 4. Results of the two-way shape memory tests at an applied prestrain of 20%, in terms of a cooling/heating cycle under mechanical load.

https://doi.org/10.1021/acs.macromol.2c01064
Macromolecules 2022, 55, 8533−8547

Table 4. Results of the Two-Way Shape Memory Testing under Applied Load

		AM (%)				
	$\varepsilon_{applied}$ (%)	$\%AM_{PCL}$	$\%AM_{PEG}$	$T_{CIE,PCL}$ (°C)	$T_{CIE,PEG}$ (°C)	RM (%)
2PCL10PEG3 :1	20.6	21.8		19.6	3.9	94.8
		95	5			
PCL10PEG3 1:1	22.5	22.2		21.9	5.9	89.8
		88	12			
PCL10PEG3 1:2	21.1	20.7		19.1	3.8	93.5
		57	43			

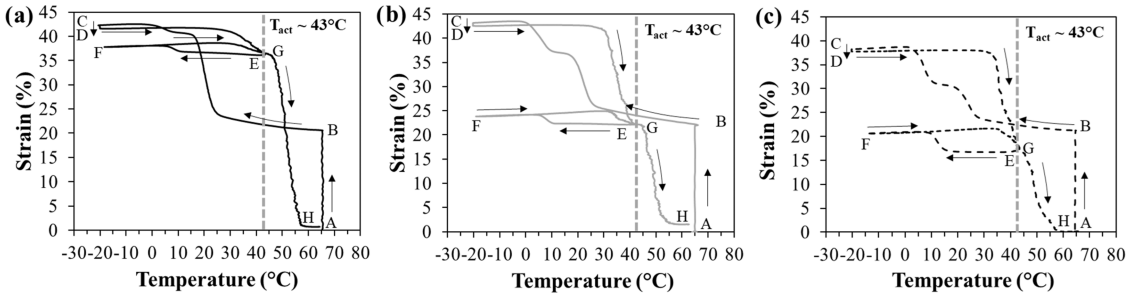

Figure 5. Reversible two-way shape memory response at T_{act} = 43 °C for (a) PCL10PEG3 2:1; (b) PCL10PEG3 1:1; and (c) PCL10PEG3 1:2 in the absence of any external load applied (from point D forward). During programming (A → B → C), a stress was applied and held constant along cooling before load removal (C → D).

thermomechanical protocol applied and the relevant structuring of the material. Upon cooling, the elongation process consists of two components:[3,5,9,13,15,16] an entropy-driven one, occurring before the crystallization takes place and consisting of the early moderate increase of strain; and a properly crystallization-driven one, occurring across the crystallization region for each phase (PCL10 and PEG3), more relevant and occurring as a steep increase that accompanies crystallization. In particular, by taking the inflection points of the curve, it was possible to evaluate the temperatures of the CIE, T_{CIE}, for each phase, resulting very close to the T_c measured by DSC. The crystallization temperature for PEG3 was found to be slightly higher compared to the DSC results for all of the networks, but this result is expected since crystallization under stretch is known to occur at higher temperatures due to the favorable alignment of the chains. The total actuation magnitude occurring over the whole cooling step, the repartition of AM between the component ascribed to PCL10 and PEG3 ($\%AM_{PCL}$ and $\%AM_{PEG}$, respectively), the temperatures of the two subelongations ($T_{CIE,PCL}$ and $T_{CIE,PEG}$), and the recovery magnitude are reported in Table 4. To evaluate $\%AM_{PCL}$ and $\%AM_{PEG}$, the following equations were used

$$\%AM_{PCL} = \frac{\varepsilon_{10°C} - \varepsilon_{applied}}{\varepsilon_{low} - \varepsilon_{applied}} \times 100 \quad (7)$$

$$\%AM_{PEG} = \frac{\varepsilon_{low} - \varepsilon_{10°C}}{\varepsilon_{low} - \varepsilon_{applied}} \times 100 = 100 - \%AM_{PCL} \quad (8)$$

where $\varepsilon_{10°C}$ is the deformation obtained at 10 °C, related to the crystallization of the PCL10 phase. AM was found to be about 20% for all of the systems, which is a value very close to the relevant $\varepsilon_{applied}$ value.

Very interestingly, in the case of these copolymeric networks, the two elongations induced upon cooling, $\%AM_{PCL}$ and $\%AM_{PEG}$, seem to be strictly related to the relative value of phase content. By way of example, when increasing the content of PEG3, from a PCL-dominant contribution to the overall AM ($\%AM_{PCL}$ is 95% of the total in the case of PCL10PEG3 2:1), the effect of the PEG3 phase becomes greater with a value of $\%AM_{PEG}$ of about 43% in PCL10PEG3 1:2, which may be considered as the network in which the contributions of the two components to the elongation were found to be similar. Upon heating, thermal expansion occurs, but the main effect is the strain reduction happening as the sum of two subprocesses, each one occurring along the thermal region corresponding to the melting of PEG3 and PCL10. This result is evident for PCL10PEG3 1:1 and 1:2, whereas for PCL10PEG3 2:1 consistent with the DMTA heating trace shown in Figure 2, the reduction of strain happens as a more continuous and smoother process. The efficient recovery of the deformation on melting, which implies the achievement of a reversible deformation under cooling/heating cycles with applied load, is indicated by the high RM values attained, close to 90% or even more.

The representation in Figure 4 is also very useful to design the protocol for the external stress-free two-way SME, mainly concerning the choice of the actuation temperature at which the reversible deformation cycle is promoted without an applied load. In fact, it is possible to identify during the heating branches, at about 43 °C, a region in which the contribution to the strain recovery of the PEG3 phase is completed, whereas the one from PCL10 is not initiated yet. Therefore, this was chosen to be the separation temperature to be leveraged when working with multicrystalline systems. For these systems, a low-melting phase (here PEG3) represents the actuation domain, i.e., the one that cyclically melts and crystallizes to induce the change in strain, whereas a high-melting phase (here PCL10) provides through its skeleton-like domain of oriented crystalline lamellae the internal stress required for the crystallization of the actuation domain upon cooling. The reversible two-way SME without applied load was thus studied with the following thermomechanical protocol, which is also highlighted in every panel of Figure 5. First, a tensile deformation equal to 20% was applied at 65 °C (A → B)

https://doi.org/10.1021/acs.macromol.2c01064
Macromolecules 2022, 55, 8533−8547

and the thus-achieved stress (890, 1180, and 1210 kPa for the 2:1, 1:1, and 1:2 networks, respectively) was held constant during cooling down to −20 °C (B → C). After stress removal (C → D), a controlled heating ramp was applied up to 43 °C (D → E), where a cooling step was applied down to −20 °C (E → F). Afterward, strain recovery was promoted with heating up to 65 °C (F → G → H).

At unloading, the deformation is almost completely maintained, i.e., above 98% of the deformation attained during cooling for all of the networks. After load removal, heating was applied and, in the region 30−43 °C, it produces a significant decrease in strain, as a consequence of the melting of PEG crystals. Depending on the content of the PEG phase, the extent of reduction in strain up to 43 °C may be significantly different. In fact, for the PCL10-rich network shown in Figure 5a, the decrease in strain is only about 5.5%, whereas it is about 20% for PCL10PEG3 1:1 shown in Figure 5b and for the PEG3-rich network it corresponds to about 24%. At 43 °C, where the melting of the PEG3 phase is completed as shown from the aforementioned results, cooling under the quasi-stress-free condition was promoted well below the crystallization temperature for the PEG phase. Interestingly, for all of the networks, during cooling, after an initial almost constant curve, a relatively modest but sharp increase in strain occurs at about 6−8 °C, as evaluated from the inflection point of the curve. This strain change is ascribed only to the crystallization of the PEG phase occurring in the absence of any external load and guided by the crystalline skeleton provided by the PCL phase. The elongation may be thus considered almost completely driven by a crystallization-driven process, whereas the entropic contribution, if any, is very modest and barely appreciable, as shown by the practically flat line in the initial elongation process upon cooling (E−F segments). The poor contribution of the entropy-related terms may be a consequence of the strongly reduced mobility of the chains under the presence of the remaining unmelted crystalline structure, whose presence may be considered in strong contrast with the conditions required for entropy elasticity.

By considering the inflection point of the curve, it is possible to define the temperature of the CIE in the reversible cycle without load, and it resulted in about 9, 8, and 6 °C for PCL10PEG3 2:1, 1:1, and 1:2, respectively. Upon heating along the melting temperature of PEG, this crystallization-induced strain is recovered and, thus, it can be considered as a fully self-standing or reversible strain ε_{rev}, which can be obtained during this two-way shape memory protocol in the absence of an external applied load. The evaluation of its entity was provided through the following equation

$$\text{reversible strain, } \varepsilon_{rev} = (\varepsilon_F - \varepsilon_E) \times 100 \quad (9)$$

where ε_F is the deformation obtained at the end of the stress-free cooling (E → F) and ε_E is the deformation at T_{act}, at the end of the melting of the PEG phase.

The reversible strain ε_{rev} was found to be about 1.9, 2.1, and 4.2% for PCL10PEG3 2:1, 1:1, and 1:2, respectively. Although relatively small in its value, it is a first clear indication of a reversible strain achieved thanks to a CIE without any external force applied, but promoted by an internal driving force exerted by the crystalline skeleton domain of PCL10. In fact, thermal contraction would occur in the opposite direction than elongation. Moreover, a clear effect of the composition of the network was found on the value of ε_{rev}. In fact, by increasing the content of the PEG phase, also the value of the reversible deformation increases with a maximum of 4.2% in the PEG-rich network (i.e., PCL10PEG3 1:2). Actually, under this thermomechanical protocol, the actuation domain is composed of the PEG phase, which is responsible for the CIE under stress-free conditions; thus, the presence of PEG as a major component results in a more pronounced deformational event during cooling. Afterward, by continuing heating above T_{act}, it is possible to melt also the PCL10 phase, this way recovering the remaining deformation imparted during the first cooling under load. To quantitatively evaluate the effectiveness of the whole recovery upon heating, the strain recovery SR was introduced with the following equation

$$\text{strain recovery, } SR = \frac{\varepsilon_D - \varepsilon_H}{\varepsilon_D} \times 100 \quad (10)$$

where ε_D is the deformation obtained at the end of the unloading stage and ε_H is the residual deformation at the end of the heating stage. All of the copolymer networks exhibited good strain recovery with values above 95%, in particular, equal to 98.2, 96.3, and 97.3% for PCL10PEG3 2:1, 1:1, and 1:2, respectively.

To verify the repeatability of the stress-free two-way reversible SME, an additional test, including three heating−cooling cycles without applied stress, was performed. The results are reported in Figure 6 for PCL10PEG3 1:2, which displays the greatest ε_{rev} value among the compositions, as measured from Figure 5. After the programming part of the test shown with a black dashed line, the stress-free reversible cycles between 43 and −15 °C are highlighted with a solid black line and plotted as the evolution of the strain as a function of time together with stress and temperature versus time curves (Figure 6) and as a function of temperature (Figure S7, Supporting Information). The three cycles were found to be completely overlapped in the strain versus temperature representation; interestingly, the cyclic stress-free thermal history in terms of the heating/cooling ramps is well evident, leading to the three cyclic evolutions of strain with a ε_{rev} value equal to 4.2% throughout the three cycles, without any loss of performance. The repeatability and reversibility of the effect were thus confirmed under a reasonable cycle number and the employed thermomechanical conditions (i.e.,

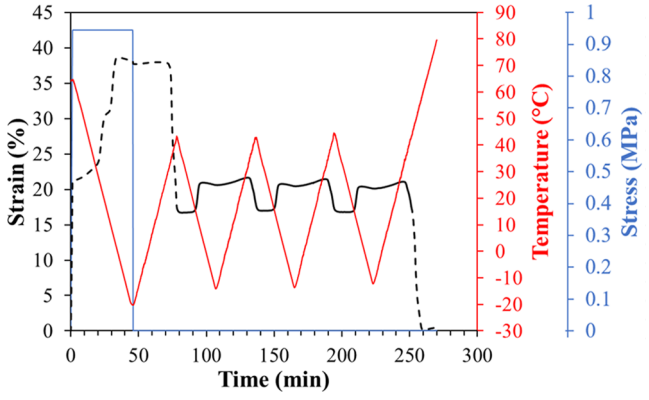

Figure 6. Results of the stress-free two-way shape memory response for PCL10PEG3 1:2 evaluated over three cycles and represented in terms of strain, temperature, and stress versus time curves. The solid line represents the three reversible cycles, the dashed line represents the programming cycle and the end of the test.

https://doi.org/10.1021/acs.macromol.2c01064
Macromolecules 2022, 55, 8533−8547

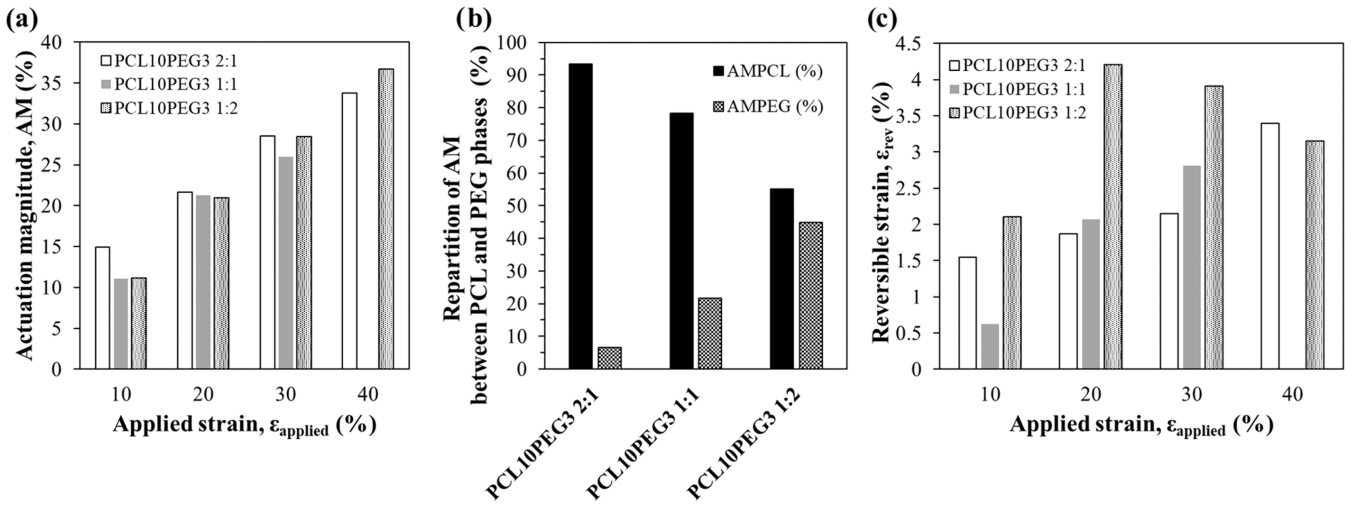

Figure 7. Evaluation of different parameters for reversible two-way shape memory tests at different applied strains $\varepsilon_{applied}$ for all of the copolymer networks, relevant to (a) actuation magnitude under load, (b) repartition of the actuation magnitude between the PCL10 and the PEG3 phases on average for the various $\varepsilon_{applied}$ values employed, and (c) extent of the reversible strain ε_{rev} achieved during reversible two-way shape memory tests without any external load applied.

all heating/cooling steps were performed at the same rate of 2 °C min^{-1}).

To better explore and try to optimize the reversible strain effect without any applied load in terms of its entity, the thermomechanical protocol applied in Figure 5 was first modified by applying different amounts of prestrain $\varepsilon_{applied}$ ranging from 10 to 40%. For PCL10PEG3 1:1, because of its less deformable behavior as demonstrated by the stress−strain curve in Figure 3, it was possible to apply a maximum of 30% strain without failure. All of the tests performed resulted in a strain−temperature curve similar in shape to the ones presented in Figure 5, and it was possible to evaluate the relevant indices plotted in Figure 7.

Figure 7a shows the dependence of the actuation magnitude on the applied prestrain, which was found to be increasingly greater for all of the networks passing from 10 to 30−40% of $\varepsilon_{applied}$. In fact, an increase in $\varepsilon_{applied}$ is accomplished by gradually greater values in the applied stress held constant in the cooling, which varies depending on the material because of the difference in stiffness previously measured. The stresses applied to obtain the same 10% strain in the materials were 470, 490, and 600 kPa for PCL10PEG3 2:1, 1:1, and 1:2, respectively, and they reached the maximum of 1497 and 1671 kPa when applying 40% strain for PCL10PEG3 2:1 and 1:2, respectively. It is known and well documented that above the minimum load of threshold for which the activation of the elongation process under crystallization takes place, the effect of a greater applied load consists of a greater elongation. This might be explained by a potential structural evolution occurring to the material during crystal formation with an increasingly higher crystallite orientation along the stretching direction as the applied stress increases. Furthermore, as noticed in Figure 5, because of the copolymeric structure of the networks, the overall elongation during cooling under load was found to be the sum of the contribution ascribed first to the formation of PCL10 crystals and for lower temperatures to those of PEG3. It was not possible to find any trend in the repartition of the actuation magnitude for different $\varepsilon_{applied}$ values given the same material; therefore, $\%AM_{PCL}$ and $\%AM_{PEG}$ were evaluated following eqs 7 and 8 as the average of the measurements obtained for different $\varepsilon_{applied}$ values for each material and presented in Figure 7b. As expected from the composition of the networks, the contribution of PCL10 to the total actuation magnitude is predominant in PCL10PEG3 2:1 with a value of $\%AM_{PCL}$ above 90%, and it is still very significant in PCL10PEG3 1:1 ($\%AM_{PCL}$ almost 80%). For PCL10PEG3 1:2, the repartition is more balanced as the two phases contributed in a similar fashion to the overall actuation magnitude, being $\%AM_{PCL}$ equal to about 55% and thus $\%AM_{PEG}$ of about 45%. Once the materials are structured and the crystals are formed and potentially aligned to the loading direction for the various $\varepsilon_{applied}$ explored, stress removal and a controlled heating ramp are activated to reach the actuation temperature for the reversible strain cycle without load (i.e., about 43 °C). At this point, a partial reduction of strain already occurred due to the complete melting of the PEG3 phase and its entity is strictly related to the composition of the networks. In fact, similar to what is reported in Figure 5, at T_{act}, the strain is reduced down to 84 ± 4, 57 ± 18, and 44 ± 9% of its value at the end of cooling (i.e., corresponding to the value of AM) on an average, for PCL10PEG3 2:1, 1:1, and 1:2, respectively. During the subsequent cooling, the steep increase in strain characteristic of the CIE occurred due to the PEG3 phase at a T_{CIE} variable depending on $\varepsilon_{applied}$. For PCL10PEG3 2:1 and 1:1 networks, T_{CIE} goes from about 7 °C at 10% $\varepsilon_{applied}$, 9 °C at 20% $\varepsilon_{applied}$, and 10 °C at 30% $\varepsilon_{applied}$, to 11 °C at 40%, whereas for PCL10PEG3 1:2, T_{CIE} was found to be quite stable at about 6 °C regardless of $\varepsilon_{applied}$. In general, the obtaining of increasingly greater values of the temperature at which the elongation takes place as the applied load increases may be expected, considering the possible increase in the crystallization temperature when happening under increasing deformation. Afterward, the variation in strain upon cooling is totally recovered upon melting up to 43 °C, and the entity of the reversible strain is measured and reported in Figure 7c. Interestingly, ε_{rev} is found to be affected for each material by the prestrain applied. $\varepsilon_{applied}$ equal to 10% is enough to produce a limited yet still appreciable reversible deformation, close to 1.5% for PCL10PEG3 2:1. The same material under 40% prestrain is capable of showing a more than doubled ε_{rev} (i.e.,

https://doi.org/10.1021/acs.macromol.2c01064
Macromolecules 2022, 55, 8533−8547

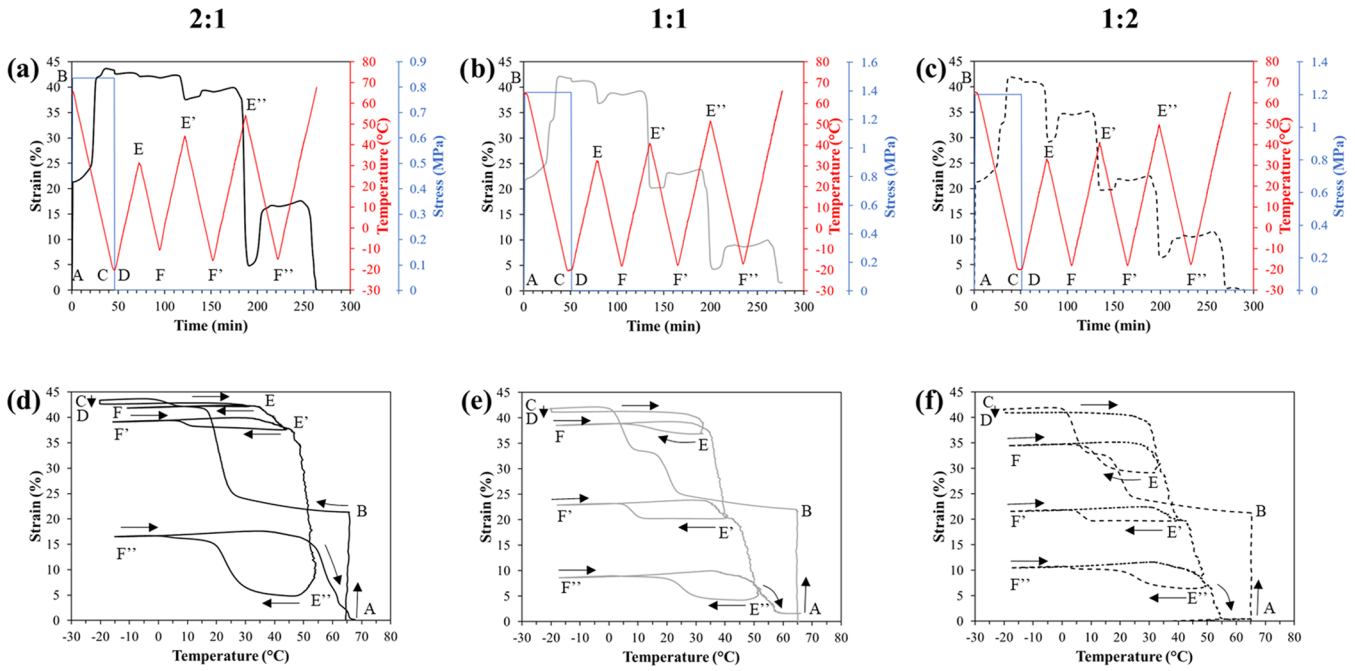

Figure 8. Evolution of the strain (black/gray/dashed black trace on the primary vertical axis), the temperature (red trace on the secondary vertical axis), and the stress (blue trace on the tertiary vertical axis) versus time for (a) PCL10PEG3 2:1, (b) PCL10PEG3 1:1, and (c) PCL10PEG3 1:2. Strain versus temperature curves for (d) PCL10PEG3 2:1 (black line), (e) PCL10PEG3 1:1 (gray line), and (f) PCL10PEG3 1:2 (black dashed line).

equal to 3.4%). For both PCL10PEG3 2:1 and 1:1, the reversible deformation is an increasing function of the applied prestrain, with a peak for the case of PCL10PEG3 1:1 after undergoing 30% prestrain, for which ε_{rev} was more than 4 times greater than in the case of $\varepsilon_{applied}$ equal to 10%. Interestingly, in the case of PCL10PEG3 1:2, after an initial increasing trend, the reversible strain slightly decreased above 30% applied prestrain. This evidence suggested that there may exist a limit beyond which an increase in $\varepsilon_{applied}$ does not result in greater ε_{rev} values. Concerning the entity of ε_{rev}, it should be noted that under this thermomechanical protocol, which makes use of the whole PEG phase as the actuation domain and the whole PCL phase as the skeleton domain, the PEG phase was found to be the sole factor responsible for the self-standing deformation, and this consideration should motivate the reason for its moderate value. In fact, depending on the specific material code and its composition, the PEG phase content is limited, and it is predominant only in PCL10PEG3 1:2, which accordingly is the network displaying the greatest value of ε_{rev}. Furthermore, not the whole PEG content is available as the actuation domain since it is a semicrystalline phase, i.e., composed of an amorphous part and a crystallizable one. The importance of the crystallinity content in determining the extent of the reversible deformation has also been reported in the work by Yang et al., in which they showed a maximum ε_{rev} of about 8% for a PEG-based network with a degree of crystallinity equal to 25.3%.[22] Therefore, our result is not surprising and may be considered an inherent limit of the capability of PEG-based actuation domains. Similar considerations may be drawn also by looking at the results of the traditional two-way shape memory tests, summarized in Table 4, in which the repartition of AM between the PCL phase and the PEG one showed that also in these conditions assisted by the presence of load, the major contribution does not come from the PEG phase but from the PCL one.

These considerations suggested exploring also other thermomechanical protocols, in which T_{act} was progressively changed to better understand the effect of the combined action of the actuation and skeleton domains. The designed thermomechanical history in terms of the imposed evolution of temperature and stress along time and the obtained evolution of strain along time are reported in Figure 8a–c, respectively, for PCL10PEG3 2:1, 1:1, and 1:2. After applying a prestrain equal to 20% at 65 °C and after performing the cooling under a fixed load, from these representations, it is possible to highlight the thermal cycles applied to the materials and underline the T_{act} of the reversible strain cycles as the peaks in the red traces, equal to 32 °C (point E), 42 °C (point E′), and 50 °C (point E″), followed by a final heating to recover the remaining deformation. For an easier readability of the results, the strain versus temperature curves are reported in the corresponding Figure 8d–f for PCL10PEG3 2:1, 1:1, and 1:2.

The curves are very similar among the three materials in the first part until the actuation of the first cooling–heating cycle without applied load at 32 °C, where the effect of the composition starts to play a role. In fact, for PCL10PEG3 2:1, no reversible strain cycle is visible being the amount of the effect similar, if even less big, to the thermal contraction and expansion, whereas a clear ε_{rev} may be identified and measured at about 2 and 5.6% with a T_{CIE} equal to about 15 and 12 °C for PCL10PEG3 1:1 and 1:2, respectively. At this T_{act}, for PCL10PEG3 2:1, the melting-induced contraction process for the PEG phase had just slightly started, suggesting that most of the PEG crystals are still intact; by contrast, the melting-induced contraction of PCL10PEG3 1:1 and 1:2 is already well developed, suggesting partial melting of the PEG phase. The elongation upon cooling occurs as a quite broad and continuous process starting at about 22 °C. Afterward, for the second cooling–heating cycle without load at 42 °C, T_{act} is

https://doi.org/10.1021/acs.macromol.2c01064
Macromolecules 2022, 55, 8533–8547

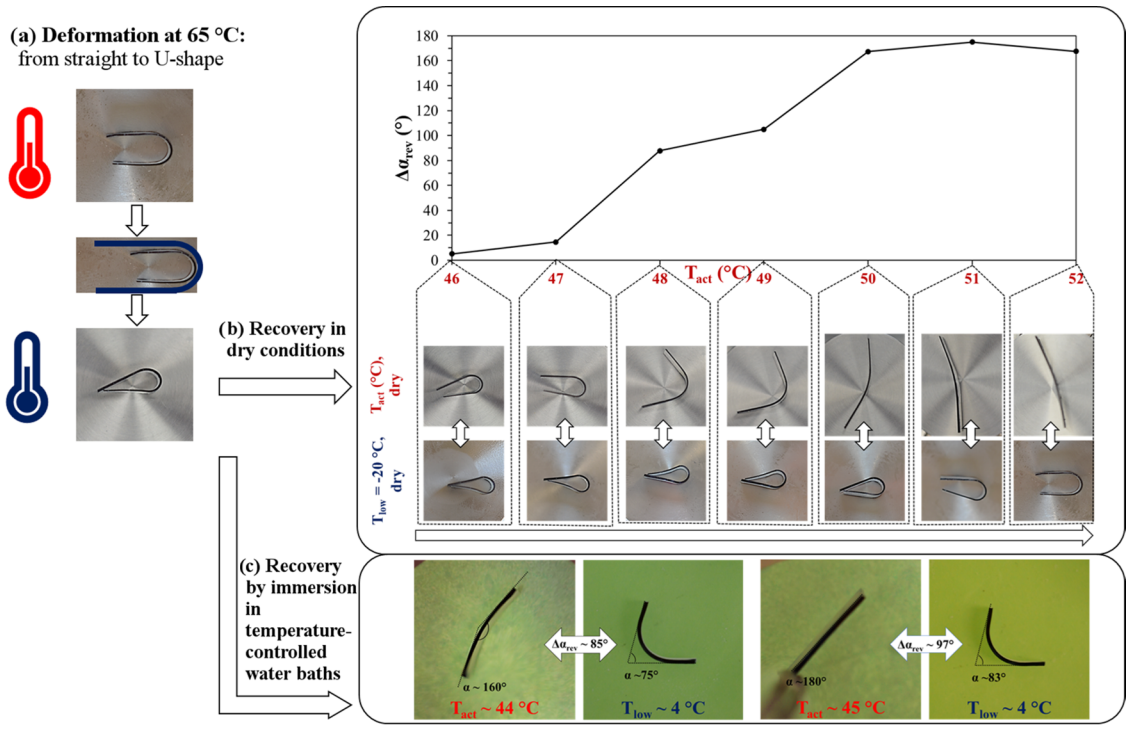

Figure 9. Reversible two-way shape memory effect in flexural experiments involving the cyclic reversible change between an I-shaped bar and a bent bar for PCL10PEG3 2:1: (a) representative picture and schematics of the procedure for fixing the U-shape; (b) recovery in dry conditions, performed by cycling the sample between T_{act} 46−52 °C and T_{low} about −20 °C; and (c) recovery by immersing the sample in temperature-controlled water baths between T_{act} 44−45 °C and T_{low} about 4 °C. Dashed lines are drawn as guide lines for measuring the angles, which are reported on the images, together with the total reversible angle $\Delta\alpha_{rev}$ obtained by cooling−heating without applied load.

located above $T_{m,PEG}$ but below $T_{m,PCL}$, i.e., in similar conditions of the test in Figure 5. Here, the reversible strain is present for all of the materials, and the values are equal to 1.9, 3, and 2.2% for PCL10PEG3 2:1, 1:1, and 1:2, respectively. The temperature at which the elongation occurs is evaluated with T_{CIE} values of about 9, 8, and 7 °C, respectively. These temperature values suggested that for these cycles the only factor responsible for the reversible deformation is the PEG phase. Eventually, for the third cycle performed at T_{act} equal to 50 °C, the materials have a totally amorphous PEG phase, whereas the PCL phase is in its melting zone. Consequently, here the mechanism for the self-standing shape memory effect should change and involve all of the PEG phases and a part of the PCL one to act as the actuation domain, which cyclically melts and crystallizes, whereas PCL crystals with T_m greater than 50 °C should provide the crystalline skeleton domain acting as a guiding force. Upon cooling, reversible deformation cycles with significant entities occurred for all of the materials. In more details, ε_{rev} is equal to 11.6, 4.5, and 4.2% for PCL10PEG3 2:1, 1:1, and 1:2, respectively, according to the decreasing percentage of the PCL phase present. Interestingly, also an entropy-driven elongation component seems to be present (segments E″−F″ in Figure 9), thanks to the higher mobility of the chains when only few crystals are present, allowing in this case a response that obeys the entropic elasticity.

Furthermore, on a closer look, the increase in strain ascribed to crystallization was found to be composed of two subprocesses, with a prevalent elongation for higher temperatures and a second, less-pronounced flex for lower temperatures. The first elongation occurred at T_{CIE} of about 24, 25, and 26 °C for PCL10PEG3 2:1, 1:1, and 1:2, respectively, and it clearly represented the prevalent contribution given by the PCL10 phase part of the actuation domain. The second inflection point is measured at about 5, 4, and 3 °C, respectively, corresponding to the crystallization of the PEG phase. This second contribution is of a significantly smaller amount, particularly of 0.6, 0.2, and 0.4% for PCL10PEG3 2:1, 1:1, and 1:2, respectively.

The stress-free reversible effect was also explored as a flexural effect by testing specimens in conditions that may be closer to applications. This additional test consisted of programming a rectangular bar in a U-shape under a fixed strain-cooling. Afterward, the U-shaped bar was partially or completely recovered, under dry conditions, up to the chosen T_{act}, ranging from 40 to 52 °C. At this point, the sample was moved to a freezer at −20 °C and, after equilibration, its change in shape was observed and recorded. Pictures of relevant timepoints of the experiments are shown in Figure 9a,b for PCL10PEG3 2:1.

From the pictures reported, the effect starts to be particularly evident at T_{act} equal to 48 °C and reaches a maximum at 51 °C, for which the completely recovered I-shaped bar is capable of changing its shape back to the initial U-shaped bar with a change in angle almost equal to 180°. Furthermore, together with the change in shape, there is also a significant change in the material's stiffness. In fact, from T_{act}, where the material is almost completely amorphous and soft, after exposure to a temperature suitable for crystallization, it crystallizes and thus becomes stiffer.

Considering the amphiphilic nature of the networks, the two-way stress-free recovery response under bending was also performed under wet conditions, by immersing the U-sample in temperature-controlled water baths, and relevant pictures

https://doi.org/10.1021/acs.macromol.2c01064
Macromolecules 2022, 55, 8533−8547

are reported in Figure 9c. This additional characterization was performed in light of future applications in the biomedical field, for which it is of utmost importance to provide a material with a stress-free reversible shape memory effect functioning also in the presence of water. Interestingly, the reversible flexural deformation is greater in dry conditions and it occurs at slightly higher temperatures (5−7 °C higher). This may be explained by the hydrophilic nature of the PEG phase, which can significantly swell in water depending on the weight content: experimental results show that for PCL10PEG3 2:1 the water uptake is around 25%, but it increases dramatically for the PEG-rich composition, i.e., about 100% for PCL10PEG3 1:2 (Figure S8, Supporting Information). Swelling plays a not negligible role in that it hinders the crystallization of PEG, as reported in the literature,[49] and therefore, the PEG phase does not contribute to the total deformation induced by the crystallization. In addition, in swollen networks, the melting temperature of the PCL phase is probably slightly lower, resulting in the activation of the recovery for lower T_{act} under wet conditions, as found in Figure 9c. Even if the reversible changes in the angle of the sample are smaller under wet conditions compared to dry ones, it is worthy to notice that PCL10PEG3 2:1 retains its noticeable reversible two-way shape memory effect also in wet conditions. Both these simple experiments clearly highlight that reversible deformation like the ones found for these materials, ranging from 4% to almost 12% under tensile conditions, may result in significant macroscopic shape changes if designed in particularly relevant sections of an object such as hinges, potentially relevant for the design and development of novel artificial muscles and reversible actuators for soft robotics and shape-shifting medical devices.[50−52]

CONCLUSIONS

Semicrystalline photo-cross-linked networks based on poly(ethylene glycol)/poly(ε-caprolactone) were synthesized with the aim of obtaining materials capable of showing a stress-free two-way SME. Various compositions of this amphiphilic network were explored and preliminarily subjected to a thermal characterization to evidence systems presenting well-separated melting and crystallization transitions of the two polymeric components. Among these systems, the most suitable were selected, i.e., copolymers based on poly(ethylene glycol) 3 kDa (PEG3) and poly(ε-caprolactone) 10 kDa (PCL10), mixed in 1:2, 1:1, and 2:1 weight ratios. A thorough thermal, mechanical, and thermomechanical characterization allowed us to properly design shape memory testing protocols and to evaluate the two-way SME under the presence of stress and in stress-free conditions. All of the materials showed excellent two-way shape memory capabilities under stress, with significant elongation−contraction effects when cyclically cooled and heated across the crystallization and melting regions. The whole crystallization-induced elongation, as well as the melting-induced contraction, consists of two subprocesses, each one ascribed to a polymeric phase, with an extent and thermal region that strongly depends on composition.

On the basis of the region of melting-contraction subprocesses, stress-free two-way shape memory testing protocols were designed, so as to evaluate the reversible deformation capability without the application of any external load. The effect was achieved by leveraging one phase as the actuation domain and the other one as the skeleton domain. The former one is the low-melting-point phase, i.e., PEG3, and it represents the phase that cyclically melts and crystallizes, thus undergoing elongation upon cooling and contraction upon melting. The latter one is the high-melting-point phase, i.e., PCL10, which, thanks to its crystalline structure, acts as an internal driving force for the elongation of the PEG phase. To rely on such micromechanisms, the most important parameter to set was the so-called actuation temperature, i.e., the maximum temperature of the cooling−heating cycle, chosen in this case in the middle between the melting-induced contraction of the PEG3 and PCL10 phases. For this well-defined and fixed actuation temperature, the maximum achieved reversible deformation is about 4.2%. However, the versatility of these materials allowed us to apply also more complex thermomechanical histories, in which different actuation temperatures and prestrains are employed, this way modifying and tuning the composition of the actuation and skeleton domains. More in details, the maximum reversible deformation that can be achieved in a cyclic history corresponds to the actuation temperature of 50 °C and it is equal almost to 12%. In addition, the reversible deformation generally increases with the applied prestrain. Therefore, by setting up suitable thermomechanical protocols, it is possible to tailor the material's response and to obtain values of the reversible deformation that are significant and may be used for applications in which a reversible deformation is needed without the assistance of any load. By way of example, we envision that these materials may prove very useful for the design of SMP-based actuators, capable of providing either reversible shape changes or cyclic forces, for building multimaterial structures with reversibly movable hinges, and to provide medical devices with a smart reversible response. All of these applications are currently being explored and attempted in the communities of soft robotics and bioengineering, and the synthesis and rational use of new shape memory polymers, such as the self-standing copolymeric networks here proposed, may prove to be highly beneficial.

ASSOCIATED CONTENT

Supporting Information

The Supporting Information is available free of charge at https://pubs.acs.org/doi/10.1021/acs.macromol.2c01064.

^{1}H NMR spectra of hydroxy and dimethacrylate PCL10 (Figure S1); ^{1}H NMR spectra of hydroxy and dimethacrylate PEG3 (Figure S2); additional DSC scans (Figures S3−S5); results of preliminary tensile tests (Figure S6); alternative representation and magnification of the repeatability of the stress-free reversible cycle for PCL10PEG3 2:1 (Figure S7); and water uptake for PCL10-PEG3 networks as a function of the weight percentage of the PEG phase (Figure S8) (PDF)

AUTHOR INFORMATION

Corresponding Author

Nicoletta Inverardi − *Department of Mechanical and Industrial Engineering, University of Brescia, 25133 Brescia, Italy; INSTM, National Interuniversity Consortium of Materials Science and Technology, 50121 Firenze, Italy;* Present Address: Department of Orthopaedic Surgery, Massachusetts General Hospital, 55 Fruit St, Boston, Massachusetts 02114, United States; orcid.org/0000-

https://doi.org/10.1021/acs.macromol.2c01064
Macromolecules 2022, 55, 8533−8547

0003-3550-9299; Email: n.inverardi003@unibs.it, ninverardi@mgh.harvard.edu

Authors

Maurizio Toselli − *Department of Industrial Chemistry "Toso Montanari", University of Bologna, 40136 Bologna, Italy; INSTM, National Interuniversity Consortium of Materials Science and Technology, 50121 Firenze, Italy*

Giulia Scalet − *Department of Civil Engineering and Architecture, University of Pavia, 27100 Pavia, Italy; INSTM, National Interuniversity Consortium of Materials Science and Technology, 50121 Firenze, Italy*

Massimo Messori − *Department of Applied Science and Technology, Politecnico di Torino, 10129 Torino, Italy; INSTM, National Interuniversity Consortium of Materials Science and Technology, 50121 Firenze, Italy*

Ferdinando Auricchio − *Department of Civil Engineering and Architecture, University of Pavia, 27100 Pavia, Italy; INSTM, National Interuniversity Consortium of Materials Science and Technology, 50121 Firenze, Italy*

Stefano Pandini − *Department of Mechanical and Industrial Engineering, University of Brescia, 25133 Brescia, Italy; INSTM, National Interuniversity Consortium of Materials Science and Technology, 50121 Firenze, Italy*

Complete contact information is available at: https://pubs.acs.org/10.1021/acs.macromol.2c01064

Author Contributions

The manuscript was written through contributions of all authors. All authors have given approval to the final version of the manuscript.

Notes

The authors declare no competing financial interest.

■ ACKNOWLEDGMENTS

This work was partially supported by the INSTM Consortium through the project "New materials and computational approaches for 4D printing". The authors would like to acknowledge Metalpres Donati Spa (Passirano (BS)—Italy) and Rubinetterie Bresciane Bonomi Spa (Gussago (BS)—Italy) for supporting this research and Mr. Gabriele Gemmo for his kind help in the experimental tests.

■ REFERENCES

(1) Lendlein, A.; Kelch, S. Shape-Memory Polymers. *Angew. Chem., Int. Ed.* **2002**, *41*, 2034−2057.

(2) Behl, M.; Lendlein, A. Shape-memory polymers. *Mater. Today* **2007**, *10*, 20−28.

(3) Chung, T.; Romo-Uribe, A.; Mather, P. T. Two-Way Reversible Shape Memory in a Semicrystalline Network. *Macromolecules* **2008**, *41*, 184−192.

(4) Lee, K. M.; Knight, P. T.; Chung, T.; Mather, P. T. Polycaprolactone−POSS Chemical/Physical Double Networks. *Macromolecules* **2008**, *41*, 4730−4738.

(5) Westbrook, K. K.; Parakh, V.; Chung, T.; Mather, P. T.; Wan, L. C.; Dunn, M. L.; Qi, H. J. Constitutive Modeling of Shape Memory Effects in Semicrystalline Polymers With Stretch Induced Crystallization. *J. Eng. Mater. Technol.* **2010**, *132*, No. 041010.

(6) Hong, S. J.; Yu, W.-R.; Youk, J. H. Two-way shape memory behavior of shape memory polyurethanes with a bias load. *Smart Mater. Struct.* **2010**, *19*, No. 035022.

(7) Zotzmann, J.; Behl, M.; Hofmann, D.; Lendlein, A. Reversible Triple-Shape Effect of Polymer Networks Containing Polypentadecalactone- and Poly(ε-caprolactone)-Segments. *Adv. Mater.* **2010**, *22*, 3424−3429.

(8) Dolynchuk, O.; Kolesov, I.; Radush, H.-J. Thermodynamic description and modeling of two-way shape-memory effect in crosslinked semicrystalline polymers. *Polym. Adv. Technol.* **2014**, *25*, 1307−1314.

(9) Scalet, G.; Pandini, S.; Toselli, M.; Messori, M.; Auricchio, F. A one-dimensional phenomenological model for the two-way shape-memory effect in semi-crystalline networks. *Polymer* **2018**, *158*, 130−148.

(10) Raquez, J.-M.; Vanderstappen, S.; Meyer, F.; Verge, P.; Alexandre, M.; Thomassin, J.-M.; Jérome, C.; Duboi, P. Design of Cross-Linked Semicrystalline Poly(ε-caprolactone)-Based Networks with One-Way and Two-Way Shape-Memory Properties through Diels−Alder Reactions. *Chem.—Eur. J.* **2011**, *17*, 10135−10143.

(11) Li, J.; Rodgers, W. R.; Xie, T. Semi-crystalline two-way shape memory elastomer. *Polymer* **2011**, *52*, 5320−5325.

(12) Behl, M.; Zotzmann, J.; Lendlein, A. One-Way and Reversible Dual-Shape Effect of Polymer Networks Based on Polypentadecalactone Segments. *Int. J. Artif. Organs* **2011**, *34*, 231−237.

(13) Pandini, S.; Baldi, F.; Paderni, K.; Messori, M.; Toselli, M.; Pilati, F.; Gianoncelli, A.; Brisotto, M.; Bontempi, E.; Riccò, T. One-way and two-way shape memory behaviour of semi-crystalline networks based on sol−gel cross-linked poly(ε-caprolactone. *Polymer* **2013**, *54*, 4253−4265.

(14) Yang, Q.; Zheng, W.; Zhao, W.; Peng, C.; Ren, J.; Yu, Q.; Hu, Y.; Zhang, X. One-way and two-way shape memory effects of a high-strain cis-1,4-polybutadiene−polyethylene copolymer based dynamic network via self-complementary quadruple hydrogen bonding. *Polym. Chem.* **2019**, *10*, 718−726.

(15) Pandini, S.; Passera, S.; Messori, M.; Paderni, K.; Toselli, M.; Gianoncelli, A.; Bontempi, E.; Riccò, T. Two-way reversible shape memory behaviour of crosslinked poly(ε-caprolactone). *Polymer* **2012**, *53*, 1915−1924.

(16) Pandini, S.; Dioni, D.; Paderni, K.; Messori, M.; Toselli, M.; Bontempi, E.; Riccò, T. The two-way shape memory behaviour of crosslinked poly(ε-caprolactone) systems with largely varied network density. *J. Intell. Mater. Syst. Struct.* **2016**, *27*, 1388−1403.

(17) Lai, S.-M.; Chen, Y.-J.; Yu, B.-Y. Preparation and characterization of two-way shape memory olefin block copolymer/silicone elastomeric blends. *J. Appl. Polym. Sci.* **2021**, *138*, No. 51238.

(18) Hao, C.; Wang, K.; Wang, Z.; Duan, R.; Liu, H.; Huang, M.; Liu, W.; He, S.; Zhu, C. Triple one-way and two-way shape memory poly(ethylene-co-vinyl acetate)/poly(ε-caprolactone) immiscible blends. *J. Appl. Polym. Sci.* **2022**, *139*, No. 51426.

(19) Meng, Y.; Jiang, J.; Anthamatten, M. Shape Actuation via Internal Stress-Induced Crystallization of Dual-Cure Networks. *ACS Macro Lett.* **2015**, *4*, 115−118.

(20) Fan, L. F.; Rong, M. Z.; Zhang, M. Q.; Chen, X. D. A facile approach toward scalable fabrication of reversible shape-memory polymers with bonded elastomer microphases as internal stress provider. *Macromol. Rapid Commun.* **2017**, *38*, No. 1700124.

(21) Saatchi, M.; Behl, M.; Nöchel, U.; Lendlein, A. Copolymer Networks From Oligo(ε-caprolactone) and n-Butyl Acrylate Enable a Reversible Bidirectional Shape-Memory Effect at Human Body Temperature. *Macromol. Rapid Commun.* **2015**, *36*, 880−884.

(22) Yang, G.; Liu, X.; Tok, A. I. Y.; Lipik, V. Body temperature-responsive two-way and moisture-responsive one-way shape memory behaviors of poly(ethylene glycol)-based networks. *Polym. Chem.* **2017**, *8*, 3833−3840.

(23) Behl, M.; Kratz, K.; Nöchel, U.; Sauter, T.; Lendlein, A. Temperature-memory polymer actuators. *Proc. Natl. Acad. Sci. U.S.A.* **2013**, *110*, 12555−12559.

(24) Zhou, J.; Turner, S. A.; Brosnan, S. M.; Li, Q.; Carrillo, J.-M. Y.; Nykypanchuk, D.; Gang, O.; Ashby, V. S.; Dobrynin, A. V.; Sheiko, S. S. Shapeshifting: Reversible Shape Memory in Semicrystalline Elastomers. *Macromolecules* **2014**, *47*, 1768−1776.

(25) Qian, C.; Dong, Y.; Zhu, Y.; Fu, Y. Two-way shape memory behavior of semi-crystalline elastomer under stress-free condition. *Smart Mater. Struct.* **2016**, *25*, No. 085023.
(26) Dolynchuk, O.; Kolesov, I.; Jehnichen, D.; Reuter, U.; Radusch, H.-J.; Sommer, J.-U. Reversible Shape-Memory Effect in Cross-Linked Linear Poly(ε-caprolactone) under Stress and Stress-Free Conditions. *Macromolecules* **2017**, *50*, 3841−3854.
(27) Yuan, W.; Liu, K.; Zhou, J.; Ni, L.; Shan, G.; Bao, Y.; Pan, P. Stress-Free Two-Way Shape Memory Effects of Semicrystalline Polymer Networks Enhanced by Self-Nucleated Crystallization. *ACS Macro Lett.* **2020**, *9*, 1325−1331.
(28) Xu, Z.-Y.; Li, L.; Shi, L.-Y.; Yang, K.-K.; Wang, Y.-Z. Effect of Self-Nucleation and Stress-Induced Crystallization on the Tunable Two-Way Shape-Memory Effect of a Semicrystalline Network. *Macromolecules* **2022**, *55*, 5104−5114.
(29) Behl, M.; Kratz, K.; Zotzmann, J.; Nöchel, U.; Lendlein, A. Reversible Bidirectional Shape-Memory Polymers. *Adv. Mater.* **2013**, *25*, 4466−4469.
(30) Wang, K.; Jia, Y.-G.; Zhu, X. X. Two-Way Reversible Shape Memory Polymers Made of Cross-Linked Cocrystallizable Random Copolymers with Tunable Actuation Temperatures. *Macromolecules* **2017**, *50*, 8570−8579.
(31) Wang, K.; Zhu, X. X. Two-Way Reversible Shape Memory Polymers Containing Polydopamine Nanospheres: Light Actuation, Robotic Locomotion, and Artificial Muscles. *ACS Biomater. Sci. Eng.* **2018**, *4*, 3099−3106.
(32) Liang, R.; Yu, H.; Wang, L.; Amin, B. U.; Wang, N.; Fu, J.; Xing, Y.; Shen, D.; Ni, Z. Triple and Two-Way Reversible Shape Memory Polymer Networks with Body Temperature and Water Responsiveness. *Chem. Mater.* **2021**, *33*, 1190−1200.
(33) Lai, S.-M.; Jiang, S.-Y. F.; Chou, H.-C.; Lin, T.-Y.; Wei, Y.-E.; Yu, B.-Y. Novel two-way multiple shape memory effects of olefin block copolymer (OBC)/polycaprolactone (PCL) blends. *Poym. Test.* **2021**, *102*, No. 107333.
(34) Qiu, Z.; Ikehara, T.; Nishi, T. Miscibility and crystallization of poly(ethylene oxide) and poly(ε-caprolactone) blends. *Polymer* **2003**, *44*, 3101−3106.
(35) Kuo, S.-W.; Lin, C.-L.; Chang, F.-C. Phase Behavior and Hydrogen Bonding in Ternary Polymer Blends of Phenolic Resin/Poly(ethylene oxide)/Poly(ε-caprolactone). *Macromolecules* **2002**, *35*, 278−285.
(36) Chuang, W-T.; Shih, K.-S.; Hong, P.-D. Kinetics of Phase Separation in Poly(ε-caprolactone)/Poly(ethylene glycol) Blends. *J. Polym. Res.* **2005**, *12*, 197−204.
(37) Li, J.; Zhang, Y.; Jiacuo, Y.; Shang, Y.; Huo, H.; Jiang, S. Miscibility and rheologically determined phase diagram of poly-(ethylene oxide)/poly(ε-caprolactone) blends. *Polym. Bull.* **2012**, *68*, 1405−1423.
(38) Nguyen-Tri, P.; Prud'homme, R. E. Crystallization and Segregation Behavior at the Submicrometer Scale of PCL/PEG Blends. *Macromolecules* **2018**, *51*, 7266−7273.
(39) Castillo, R. V.; Müller, A. J. Crystallization and morphology of biodegradable or biostable single and double crystalline block copolymers. *Prog. Polym. Sci.* **2009**, *34*, 516−560.
(40) Palacios, J. K.; Mugica, A.; Zubitur, M.; Müller, A. J.Crystallization and Morphology of Block Copolymers and Terpolymers With More Than One Crystallizable Block. In *Crystallization in Multiphase Polymer Systems*; Elsevier Inc., 2018; Chapter 6, pp 123−180.
(41) He, C.; Sun, J.; Zhao, T.; Hong, Z.; Zhuang, X.; Chen, X.; Jing, X. Formation of a Unique Crystal Morphology for the Poly(ethylene glycol)−Poly(ε-caprolactone) Diblock Copolymer. *Biomacromolecules* **2006**, *7*, 252−258.
(42) He, C.; Sun, J.; Deng, C.; Zhao, T.; Deng, M.; Chen, X.; Jing, X. Study of the Synthesis, Crystallization, and Morphology of Poly(ethylene glycol)−Poly(ε-caprolactone) Diblock Copolymers. *Biomacromolecules* **2004**, *5*, 2042−2047.
(43) Piao, L.; Dai, Z.; Deng, M.; Chen, X.; Jing, X. Synthesis and characterization of PCL/PEG/PCL triblock copolymers by using calcium catalyst. *Polymer* **2003**, *44*, 2025−2031.
(44) Sun, J.; He, C.; Zhuang, X.; Jing, X.; Chen, X. The crystallization behavior of poly(ethylene glycol)-poly(ε-caprolactone) diblock copolymers with asymmetric block compositions. *J. Polym. Res.* **2011**, *18*, 2161−2168.
(45) Messori, M.; Degli Esposti, M.; Paderni, K.; Pandini, S.; Passera, S.; Riccò, T.; Toselli, M. Chemical and thermomechanical tailoring of the shape memory effect in poly(ε-caprolactone)-based systems. *J. Mater. Sci.* **2013**, *48*, 424−440.
(46) Li, Y.; Liu, R.; Huang, Y. Synthesis and phase transition of cellulose-graft-poly(ethylene glycol) copolymers. *J. Appl. Polym. Sci.* **2008**, *110*, 1797−1803.
(47) Crescenzi, V.; Manzini, G.; Calzolari, G.; Borri, C. Thermodynamics of fusion of poly-β-propiolactone and poly-ε-caprolactone. comparative analysis of the melting of aliphatic polylactone and polyester chains. *Eur. Polym. J.* **1972**, *8*, 449−463.
(48) Bogdanov, B.; Vidts, A.; Van Den Bulcke, A.; Verbeeck, R.; Schacht, E. Synthesis and thermal properties of poly(ethylene glycol)-poly(ε-caprolactone) copolymers. *Polymer* **1998**, *39*, 1631−1636.
(49) Baker, R. M.; Henderson, J. H.; Mather, P. T. Shape memory poly(3-caprolactone)-co-poly(ethylene glycol) foams with body temperature triggering and two-way actuation. *J. Mater. Chem. B* **2013**, *1*, 4916−4920.
(50) Scalet, G. Two-Way and Multiple-Way Shape Memory Polymers for Soft Robotics: An Overview. *Actuators* **2020**, *9*, No. 10.
(51) Zhao, Y.; Peng, K.; Xi, J.; Shahab, S.; Mirzaeifar, R. Achieving multimodal locomotion by a crosslinked poly(ethylene-co-vinyl acetate)-based two-way shape memory polymer. *Smart Mater. Struct.* **2022**, *31*, No. 015034.
(52) Lendlein, A.; Gould, O. E. C. Reprogrammable recovery and actuation behaviour of shape-memory polymers. *Nat. Rev. Mater.* **2019**, *4*, 116−133.

https://doi.org/10.1021/acs.macromol.2c01064
Macromolecules 2022, 55, 8533−8547